Quaternary Science Reviews 81 (2013) 74–89

Contents lists available at ScienceDirect

Quaternary Science Reviews

journal homepage: www.elsevier.com/locate/quascirev

Late Holocene glacial history of the Copper River Delta, coastal south-central Alaska, and controls on valley glacier fluctuations

David J. Barclay [a,*], Elowyn M. Yager [b], Jason Graves [a], Michael Kloczko [a], Parker E. Calkin [c]

[a] Geology Department, SUNY Cortland, Cortland, NY 13045, USA
[b] Center for Ecohydraulics Research, Department of Civil Engineering, University of Idaho, Boise, ID 83702, USA
[c] INSTAAR, University of Colorado at Boulder, Boulder, CO 80309, USA

ARTICLE INFO

Article history:
Received 10 May 2013
Received in revised form
28 September 2013
Accepted 1 October 2013
Available online

Keywords:
Valley glacier
Tree-rings
Solar irradiance
Little Ice Age
Medieval Warm Period
First Millennium A.D.
Holocene
Alaska

ABSTRACT

Fluctuations of four valley glaciers in coastal south-central Alaska are reconstructed for the past two millennia. Tree-ring crossdates on 216 glacially killed stumps and logs provide the primary age control, and are integrated with glacial stratigraphy, ages of living trees on extant landforms, and historic forefield photographs to constrain former ice margin positions. Sheridan Glacier shows four distinct phases of advance: in the 530s to *c*.640s in the First Millennium A.D., and the 1240s to 1280s, 1510s to 1700s, and *c*.1810s to 1860s during the Little Ice Age (LIA). The latter two LIA advances are also recorded on the forefields of nearby Scott, Sherman and Saddlebag glaciers. Comparison of the Sheridan record with other two-millennia long tree-ring constrained valley glacier histories from south-central Alaska and Switzerland shows the same four intervals of advance. These expansions were coeval with decreases in insolation, supporting solar irradiance as the primary pacemaker for centennial-scale fluctuations of mid-latitude valley glaciers prior to the 20th century. Volcanic aerosols, coupled atmospheric-oceanic systems, and local glacier-specific effects may be important to glacier fluctuations as supplemental forcing factors, for causing decadal-scale differences between regions, and as a climatic filter affecting the magnitude of advances.

1. Introduction

Valley glacier fluctuations are a key record for understanding the natural forcings and spatial expression of late Holocene climate change. Termini of valley glaciers respond within years to decades of a change in climate by advancing or retreating (Jóhannesson et al., 1989; Raper and Braithwaite, 2009), and leave characteristic sediments and landforms as records of past termini positions. Dates on trimlines and moraines reveal when termini reached and receded from maxima, while forefield organic materials interbedded with or incorporated into glacigenic sediments constrain intervals of ice minima and re-advance. When dated by tree-ring crossdates, these glacier forefield records have enabled termini fluctuations over the last one to two millennia to be reconstructed with very high spatial and temporal detail (e.g. Luckman, 1995; Holzhauser et al., 2005; Barclay et al., 2009a).

While valley glacier histories have been developed for many mountain areas of the world (Davis et al., 2009), there remains uncertainty as to what climatic forcings have been the dominant cause of termini fluctuations prior to the twentieth century. Some authors have emphasized solar irradiance as the primary driver (e.g. Denton and Karlén, 1973; Wiles et al., 2004; Hormes et al., 2006) while others have linked past glacier fluctuations to volcanic activity, changes in atmospheric–oceanic systems, and feedbacks such as sea ice formation (e.g. Porter, 1986; Denton and Broecker, 2008; Licciardi et al., 2009; Schaefer et al., 2009; Miller et al., 2012; Putnam et al., 2012; Lowell et al., 2013). Further interpretive complications arise from local factors such as glacier size, geometry, debris cover, and terminal environment (e.g. Pelto and Hedlund, 2001; Boyce et al., 2007; Kirkbride and Winkler, 2012), which can influence the specific response of ice margins to climatic forcing.

In this paper we use tree-ring crossdates to detail the late Holocene history of four valley glaciers that terminate on the Copper River Delta in coastal south-central Alaska. One of these records, that of Sheridan Glacier, spans almost 2000 years and is the most complete and best-constrained valley glacier history yet developed in Alaska. These data are then used to consider the relative roles of global to regional climate forcing factors and non-climatic local effects on valley glacier histories.

* Corresponding author. Tel.: +1 607 753 2921.
E-mail address: david.barclay@cortland.edu (D.J. Barclay).

0277-3791/$ – see front matter © 2013 Elsevier Ltd. All rights reserved.
http://dx.doi.org/10.1016/j.quascirev.2013.10.001

1.1. Study area

The Copper River Delta is a low relief foreland situated between Prince William Sound and the mouth of the Copper River (Fig. 1). The four study glaciers (Table 1) all flow southwards from an area of Paleogene-age sedimentary and granitoid rocks (Winkler and Plafker, 1993) in the Chugach Mountains. Peaks around the névés of the four glaciers are generally around 1200 m and locally reach to 1909 m above sea level. Sheridan and Saddlebag glaciers both currently terminate in proglacial lakes that are dammed by late Holocene moraines and associated deposits, while Scott and Sherman glaciers are fronted by vigorous outwash river systems.

Climate on the Copper River Delta is maritime with mean monthly temperatures of −4.1 °C in January and 12.5 °C in July (1971–2000, NCDC normals) being recorded at the Cordova Airport (Fig. 1). Average annual precipitation is 2445 mm and is distributed throughout the year with a peak in September and October. Climax forests on outwash are usually dominated by Sitka spruce (*Picea sitchensis* (Bong.) Carr.) and western hemlock (*Tsuga heterophylla* (Raf.) Sarg.), while mountain hemlock (*Tsuga mertensiana* (Bong.) Carr.) is generally more common on moraines, hillslopes and at higher elevations. Sitka alder (*Alnus crispa* (Ait.) Pursh ssp. *sinuata* (Reg.) Hult.) and black cottonwood (*Populus trichocarpa* Torr. & Gray) dominate early successional stages on recently disturbed or deglaciated ground (Boggs, 2000).

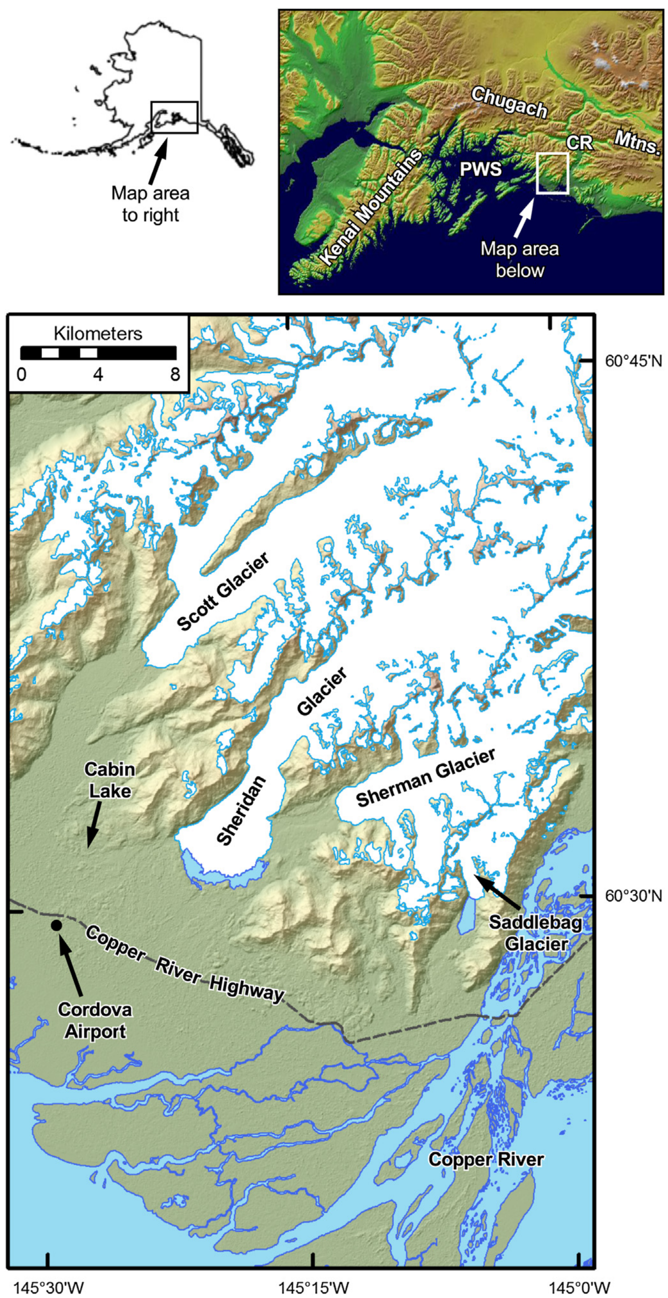

Fig. 1. Copper River Delta study area. PWS: Prince William Sound. CR: Copper River.

Table 1
Copper River Delta glacier characteristics.

Name	Length (km)	Terminus elevation (m)	Main flow direction
Scott	24	150	SW
Sheridan	24	50	SW–SSW
Sherman	13	120	WSW
Saddlebag	8	85	S

The Copper River Delta is located above the Aleutian megathrust and was co-seismically uplifted about two meters during the 1964 M9.2 earthquake (Plafker, 1969). Previous large earthquakes about 800 and 1500 years ago (Hutchinson and Crowell, 2007; Shennan et al., 2008) may have similarly uplifted the area, while drowned tree stumps at the seaward edge of the delta record gradual land surface subsidence during inter-seismic periods (Plafker, 1990). The glacier forefields of this study are high enough above sea level and sufficiently dominated by glacial processes so as to have minimal influences in the stratigraphic and landform record from vertical tectonic displacements. However, co-seismic landslides such as the 1964 large volume rock avalanche onto Sherman Glacier (Shreve, 1966) can potentially alter mass balance and thus affect glacier dynamics (Bull and Maranguanic, 1968).

1.2. Previous studies

The study glaciers were first described and sketched from a distance by expeditions traveling along the Copper River Delta shoreline in 1884 (Abercrombie, 1900) and 1886 (Seton-Karr, 1887). Although the earliest glacier maps erroneously show Sheridan and Sherman as two tributaries feeding a single terminus (Brooks, 1908; Grant and Higgins, 1909), closer observations in 1910 (Tarr and Martin, 1914) established that these were two separate glaciers and this is reflected on maps thereafter (e.g. Chapin, 1913). Tarr and Martin (1914) also noted that both Sheridan and Saddlebag glaciers were thinning and beginning to retreat from recent maxima. At Sheridan Glacier this marginal retreat amounted to 335 m from a major moraine and forest trimline by 1925–26 (Lutz, 1930), and in 1931 Wentworth and Ray (1936) noted further retreat and thinning.

Lutz (1930) examined the reforestation process on recently deglaciated ground at Sheridan Glacier and found the pioneer species to be spruce, mountain hemlock, alder and cottonwood. Both tree ages on moraines and radiocarbon ages from glacially killed stumps and logs were used by Tuthill et al. (1968) to develop a late Holocene history of Sheridan and Sherman glaciers. Field (1975) used the observations of earlier workers together with aerial photographs to summarize retreat of all four of the study glaciers from the early to middle 20th century. We incorporate key results from these prior workers with our own data in our reconstructed histories of the forefields.

2. Methods

Fieldwork for this study was completed in the summers of 1993, 1999, and 2002. Living trees and recently logged stumps on moraines and outwash surfaces, at forest trimlines, and in old growth forests beyond the forefields (Fig. 2) were cored to respectively provide dates of ice retreat, dates of ice maxima, and tree-ring series for crossdating with subfossil tree-ring samples. Sediments revealed in stream-cut exposures were documented and subfossil wood samples (Fig. 2) collected as cores or discs from the lower trunk or best-preserved section of each log or *in situ* stump. Samples for radiocarbon dating were also collected from organic horizons and some subfossil logs.

In the laboratory, wood samples were air-dried, glued, and sanded with progressively finer sandpapers to clearly reveal the tree ring and wood cell structures. Conifer samples were classified as spruce or hemlock based on the respective presence or absence of resin canals on the sanded cross-sectional surface (Hoadley, 1990). The outer edges of each subfossil wood sample were examined for the presence of bark or a pristine outer ring (i.e. minimal rot or abrasion), indicating that no outer rings had been lost after tree death. Innermost rings of all living and subfossil samples were also examined for the pith or significant ring curvature, indicating that the sample included the oldest rings at the tree center. Ring widths were measured to the nearest 0.001 mm using a Velmex linear encoder system.

Crossdating of subfossil samples was a two step-process. First, samples were matched with samples of the same genera from the same site or stratigraphic level to produce local floating chronologies. Second, these chronologies were crossdated with each other, with living trees from forests surrounding the forefields, and with master tree-ring chronologies from Nellie Juan (Barclay et al., 2003), Tebenkof (Barclay et al., 2009a), and Columbia (Wilson et al., 2007) glaciers to form final chronologies for the Copper River Delta that were calendar-dated throughout. All crossdates were made both statistically using the program COFECHA (Holmes, 1983) and by visual comparison of line graphs and core samples. Crossdating was also used to confirm ring counts of key living tree samples from moraines and outwash surfaces, and to provide felling dates for clear-cut areas where some ring counts had been made on exposed tree stump surfaces.

First and last ring dates were determined for each subfossil stump or log that had yielded ring width data that crossdated. Incomplete, distorted, and badly damaged rings had been avoided during measurement, but were included in the individual stump or log age spans when they could be counted with confidence. As a result, some stumps and logs have first and last ring dates that are earlier or later than the age spans of the final tree-ring chronologies. Cores and discs had also been collected from some subfossil logs found as driftwood around lakeshores and rivers; these samples were used for developing the tree-ring chronologies but were otherwise not interpreted.

Best estimates of the stabilization date of late Holocene moraines and outwash surfaces were based on the germination year of the oldest living or recently logged tree found on the landform. These best estimates include an ecesis time, which was subtracted

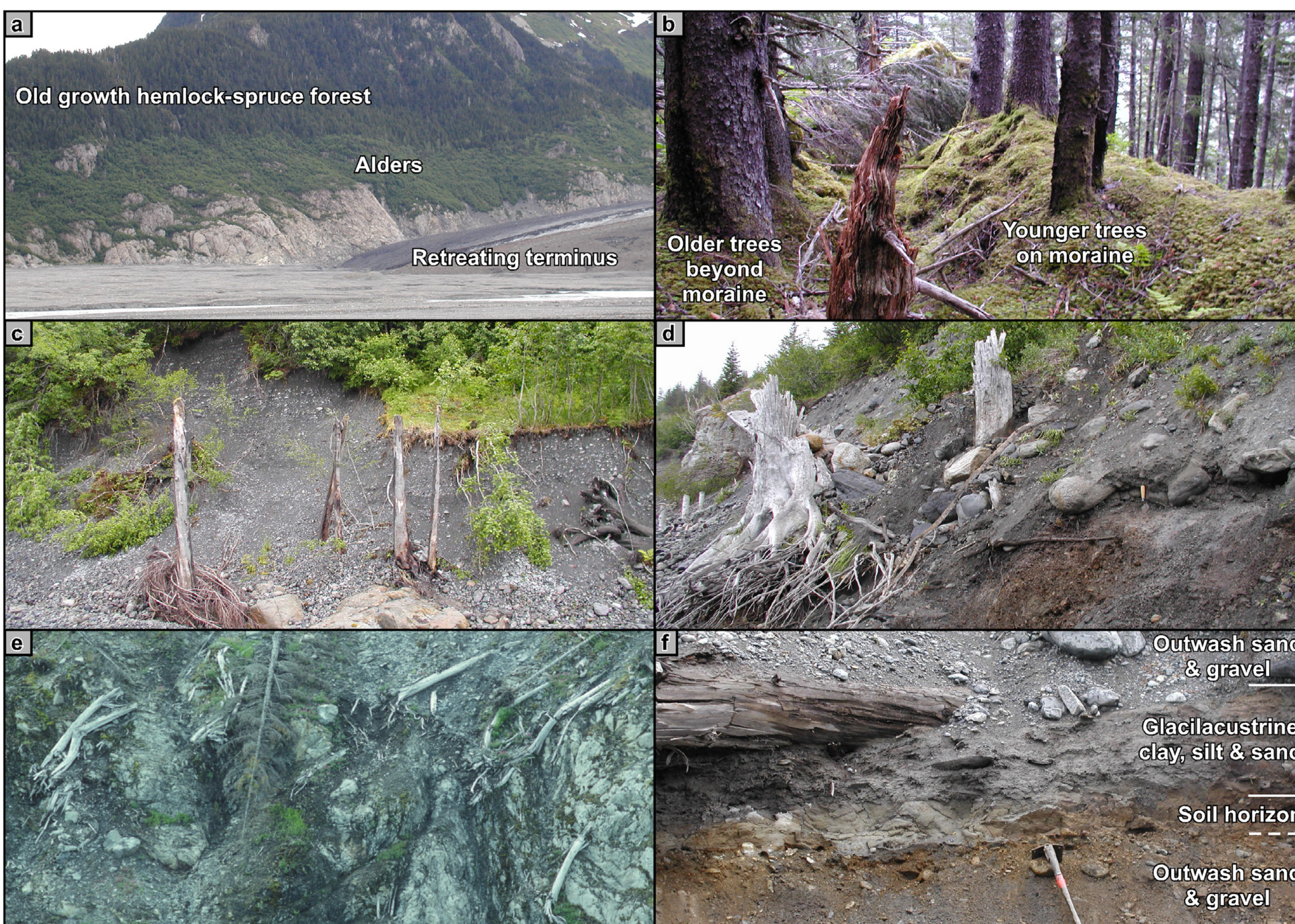

Fig. 2. Examples of field data. (a) Forest trimline at west side of Scott Glacier. (b) Forest trimline and lateral moraine at northeastern margin of Sheridan forefield. (c) *In situ* stumps recently exhumed from outwash at site C. (d) *In situ* stumps rooted on buried hillside at site N. (e) Logs crushed against bedrock at site E. (f) Transported log at site K.

from innermost ring dates to account for the elapsed time between landform stabilization and the successful germination and survival of seedlings on the surface. Based respectively on Tuthill et al. (1968) and Helm and Allen (1995), the ecesis estimates were ten years for conifers and six years for cottonwoods. Age-height corrections were also used when basal flare or other field issues required ring counts to be made above the germination point or base of the trunk. Estimates of growth rates near sea level around the northern Gulf of Alaska vary from as high as 20 cm a^{-1} for Sitka spruce growing on sand and gravel at Icy Bay (Barclay et al., 2001) to as low as 0.25 cm a^{-1} for the same species growing on an exposed till slope at Sheridan Glacier (Lutz, 1930). Tuthill et al. (1968) used a rate of 12 cm a^{-1} as an average value for the Sheridan and Sherman area and we used this rate for all four forefields.

Stabilization age estimates for buried land surfaces were similarly based on the innermost ring date of the oldest *in situ* stump. However, sampling along these buried surfaces was restricted to active stream-cut exposures and so was much less thorough than sampling of the modern land surface where we could search for and core all old-looking trees. Also, the roots of some *in situ* stumps were buried an unknown depth below the sampling height and some buried forest horizons may not have been first-generation forests on glacigenic substrates. Therefore, stabilization ages of buried land surfaces are presented herein as minimum estimates rather than best estimates, and do not include age–height or ecesis corrections. Substrate ages in old growth forests surrounding the forefields are also presented as minimum estimates because the senile age limit of spruce and hemlock (typically 500–600 years) is much younger than the probable substrate ages (1000s of years).

Seven radiocarbon ages obtained during our work and nine ages from Tuthill et al. (1968) were used as independent verification of our tree-ring crossdates and to provide additional age control. All 16 samples were calibrated using the IntCal09 calibration curve of Reimer et al. (2009) in the program CALIB 6.1.0 (Stuiver and Reimer, 1993).

Locations and elevations in the field were recorded with GPS and a barometric altimeter. A Geographic Information System (ArcGIS 10.1) was subsequently used to overlay all GPS waypoints onto topographic maps and 1996 orthophotographs to verify locations, and topographic map contours and a 2006 satellite-based digital elevation model were used to verify elevations. Changes in ice margins and forefield geomorphology over recent decades were determined from U.S. Geological Survey aerial photographs and Landsat imagery.

3. Results

3.1. Tree-ring crossdates

A total of 216 subfossil stumps and logs were crossdated and form the basis of master chronologies for spruce and hemlock for the Copper River Delta (Fig. 3). Living trees used in these chronologies were growing on moraines and proximal outwash on the southwestern Sheridan forefield, and also on moraines, outwash, and bedrock in the valley between Sheridan and Sherman glaciers. The spruce chronology spans A.D. 235–599 and 933–2001 while the hemlock chronology spans A.D. 114–608 and 838–2001. Correlations between these chronologies and other master chronologies for Prince William Sound are all significant at well above the 99% confidence level (Table 2). The coherence of the spruce chronology with the hemlock chronologies reflects the similar dendroclimatic response of these taxa in the Gulf of Alaska region (Wiles et al., 1998).

Radiocarbon results (Table 3) support the tree-ring crossdates. AMS ages on two individual growth rings (samples CURL-5294 and CURL-5298) have two standard deviation ranges that encompass the crossdates of the respective rings. Samples of bark and outer rings from three other stumps (β-98,985, β-98,986 and β-93,992) are also consistent with crossdates from the same stumps. Six other radiocarbon samples (I-1689, I-1984, I-1691, I-1690, I-1693, and I-1692) cannot be linked directly to specific crossdated stumps or logs, but are generally similar in age to subfossil wood crossdates from the same locations.

Comparison of the tree-ring crossdates and radiocarbon ages shows that the former provide more information (a span of growth with dates for both first and last years of each tree) and are also much higher precision. Accordingly, we emphasize tree-ring crossdates in reconstructing the glacier histories and only use radiocarbon ages where there are no tree-ring data for age control.

3.2. Scott Glacier

The late Holocene maximum of Scott Glacier is marked by a forest trimline (Fig. 2a) and discontinuous moraine ridges on a mountain spur on the northwest side of the forefield (Fig. 4). In the center and southeast side of the valley, alder-covered outwash terraces are graded to this same ice marginal position and respectively have kettles and a distinct outwash head to mark the former ice limit. Modern outwash streams have incised through these terraces on both sides of the valley.

Six subfossil logs were found crushed against bedrock and on active colluvial fans at the base of the mountain spur at site A (Fig. 4), and a seventh was found still rooted in growth position in the adjacent outwash. Crossdates show that these trees were alive from at least 1558 to 1838 (Fig. 3). A radiocarbon age of 1750 cal. A.D. on organic materials from a soil buried by till nearby (β-80,512, Table 3) is consistent with this same period of forest growth. Collectively these results show that the northwestern margin of Scott Glacier advanced over this site after 1838 and that tree growth here had been uninterrupted for at least the previous 280 years.

On the southeastern side of the forefield, five *in situ* stumps at site B (Fig. 4) record growth from 1435 to 1845 while 17 *in situ* stumps at site C collectively grew from 1526 to 1867. All of these stumps protrude through or were recently exhumed from the outwash terrace at the edge of the valley (Fig. 2c). Samples with bark or well preserved outer rings, as well as the overall concordance of outer ring dates (Fig. 3), suggest that pulses of outwash aggredation killed these trees from the 1840s to 1860s. In addition, four of the stumps at site B have pith dates in the 1710s, suggesting that an earlier pulse of outwash aggradation at this locale may have provided a fresh substrate on which a distinct cohort of trees germinated.

The oldest living tree found on the outermost moraine on the northwestern side of the forefield indicates ice retreat and moraine stabilization in 1904. Much older forest is present beyond the trimline, with one tree higher on the mountain spur having been alive since at least 1497. Aerial photographs taken in 1938 show some terminus thinning and retreat, and marginal retreat has been relatively continuous through the rest of the 20th century. By 2000 the northwest and southeast sides of the terminus were respectively about 1.3 and 0.7 km from the *c*.1904 maximum position.

3.3. Sheridan Glacier – southern forefield

The lobate terminus of Sheridan Glacier is rimmed on its southern side by multiple end moraine ridges and associated outwash (Fig. 5). These late Holocene deposits form the shore of the proglacial lake that currently fronts the terminus, and have been incised by meltwater at Sheridan River and the now abandoned

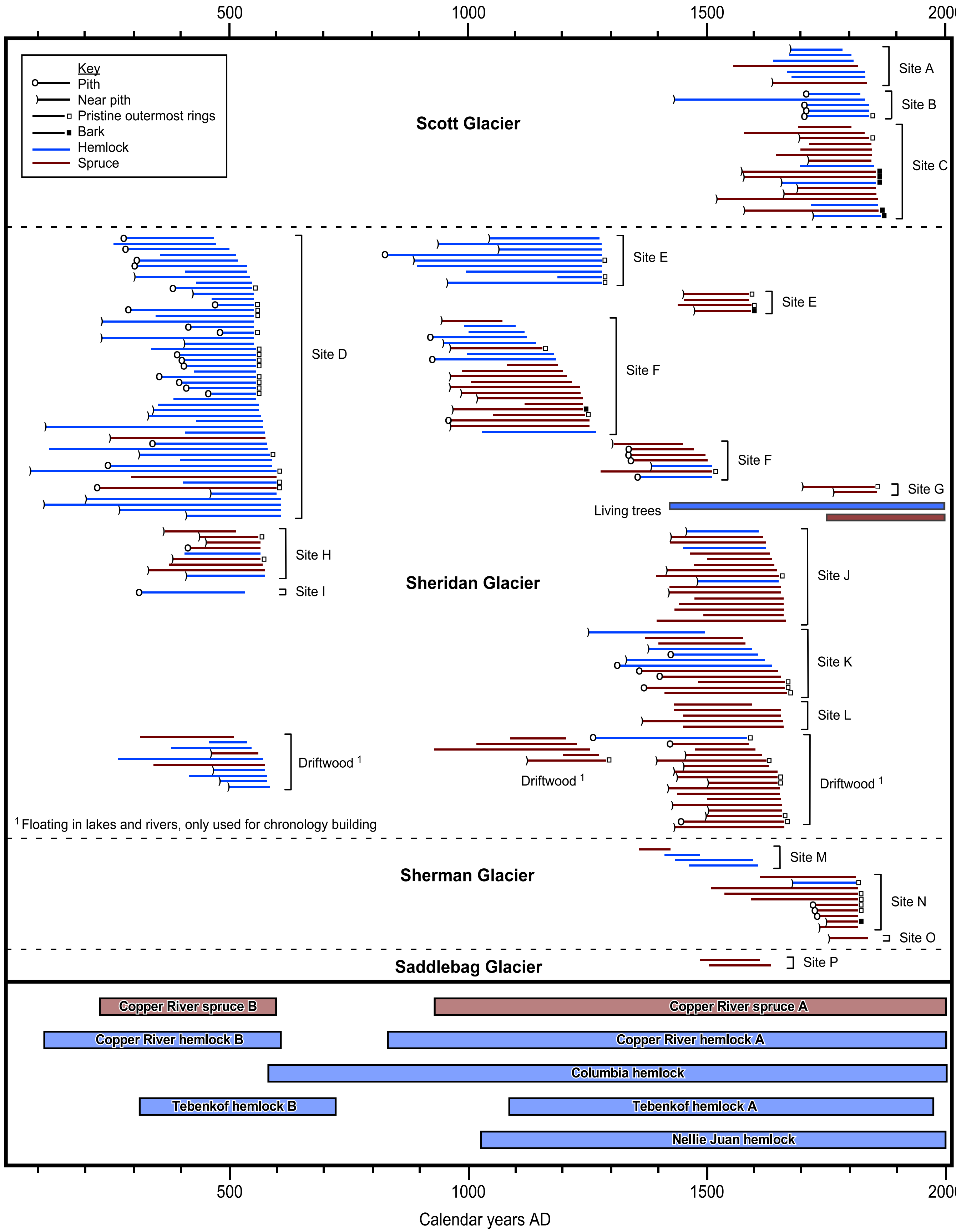

Fig. 3. Crossdated subfossil samples (upper panel) and master tree-ring chronologies (lower panel). Thin horizontal bars represent individual stumps or logs and show full interval of recorded growth. Broader horizontal blocks represent multiple trees and master chronologies. Columbia chronology: Wilson et al. (2007). Tebenkof chronology: Barclay et al. (2009a). Nellie Juan chronology: Barclay et al. (2003).

Table 2
Correlation coefficients (upper left) and years of overlap (lower right) for master tree-ring chronologies.

	NJH	TEB	COL	CRH	CRS
CRS	0.431	0.422	0.532	0.551	–
CRH	0.525	0.498	0.595	–	1418
COL	0.601	0.541	–	1176	1072
TEB	0.650	–	1174	1326	1317
NJH	–	952	952	952	952

NJH – Nellie Juan hemlock; TEB – Tebenkof hemlock; COL – Columbia hemlock; CRH – Copper River Delta hemlock; CRS – Copper River Delta spruce.

Glacier River. A prominent lateral moraine marks the former ice limit on the mountainside west of the glacier.

The oldest organic material dated at Sheridan Glacier is a log with a radiocarbon age of 1020 cal. B.C. (2970 cal. yr. BP, I-1985, Table 3). This was found in the southeastern area of the forefield by Tuthill et al. (1968) in lake sediments with abundant plant fragments, and was overlain by outwash gravel and till. However, the exact location of the site was reported as two different places in the original publication and we were unable to relocate and examine the deposit during our fieldwork.

The oldest crossdated wood was found at site D (Fig. 5) where 51 logs and *in situ* stumps collectively record continuous forest growth from A.D. 86 to 609 (Fig. 3). All but three of these samples were hemlock and at least five were over 400 years old when they died, which is a species composition and age distribution suggestive of an old growth forest that had been growing for many centuries rather than a first generation forest on relatively recent glacigenic deposits. Surrounding stratigraphy and last years of growth for *in situ* stumps with bark or pristine outer rings show that pulses of outwash aggradation killed many of these trees from the 550s to 601. Interbedded outwash and till containing transported logs overlies the *in situ* stumps, and show that the margin of Sheridan Glacier advanced over this area in or soon after 609. This First Millennium A.D. advance is also recorded on the southeastern side of the forefield by logs pushed against bedrock (Tuthill et al., 1968), one of which returned a radiocarbon age of 440 cal. yr. A.D. (I-1986, Table 3).

Subsequent retreat of the ice margin is recorded by forest growth on a bedrock knob at site E by 832 and on the nearby outwash at site F by 928 (Figs. 3 and 5). A radiocarbon age of 890 cal. yr. A.D. (I-1987, Table 3) from an *in situ* stump exposed by the former Glacier River (Tuthill et al., 1968) shows forest growth at the western edge of the forefield during this same interval. This forest growth interval ended with renewed ice advance that is first recorded by outwash aggradation at site F. One sample with a seemingly well-preserved outer edge had an outer ring date of 1156; however, additional pristine samples showing tree death at this time are needed to confirm this as an interval of widespread outwash aggradation. Clearer evidence for outwash aggradation ahead of the advancing ice margin comes from well-preserved *in situ* stumps whose kill-dates cluster from 1240 to 1269 (Fig. 3). This advance is also recorded by trees with last years of growth of 1279–1284 at nearby site E, which were killed by direct contact with Sheridan Glacier as it expanded against the bedrock knob (Fig. 2e).

This phase of advance did not reach as far as site F where trees were growing again on outwash by 1279 (Fig. 6), and retreat of the ice margin from the bedrock knob occurred before trees germinated at site E by 1442 (Fig. 3). Sheridan Glacier was advancing again in the 1510s when outwash aggradation killed and buried trees at site F, and the ice margin crushed more trees against bedrock at site E in 1593 and 1594. This advance continued over subsequent decades, depositing till over site F, and culminated with

Table 3
Radiocarbon results for Copper River Delta glacier forefields.

Lab. No.[a]	Age (BP)[b]	Calibrated age[c] (cal. yr. B.C./A.D.)	Description	Source[d]
Scott Glacier				
β-80,512	220 ± 50	1520 (1750) 1950	Site A. Organic material in soil beneath till.	2
Sheridan Glacier				
I-1985	2830 ± 100	−1290 (−1020) −810	Southeast forefield in moraine belt. Log in lake sediment under outwash and till.	1
CURL-5294	1670 ± 75	180 (370) 560	Site D. Single growth ring from same *in situ* stump as CURL-5298, ring crossdated as A.D. 311.	2
CURL-5298	1670 ± 40	250 (370) 530	Site D. Single growth ring from same *in situ* stump as CURL-5294, ring crossdated as A.D. 432.	2
I-1986	1610 ± 100	230 (440) 640	Southeast forefield in moraine belt. Log jammed against north-facing bedrock.	1
I-1987	1130 ± 100	670 (890) 1150	Glacier River in moraine belt. *In situ* stump buried in outwash.	1
β-98,985	800 ± 60	1050 (1220) 1290	Site F. Outer rings of *in situ* stump, crossdated age span of stump A.D. 933–1185.	2
I-1689	650 ± 120	1050 (1330) 1480	Sheridan River near site F. *In situ* stump buried in outwash and till.	1
I-1984	550 ± 95	1270 (1380) 1620	Sheridan River near site F. *In situ* stump buried in till of outermost Holocene moraine.	1
I-1691	480 ± 125	1270 (1450) 1800	Sheridan River near site F. *In situ* stump buried in outwash.	1
I-1690	455 ± 125	1280 (1480) 1950	Sheridan River near site F. *In situ* stump buried in outwash and till.	1
I-1693	370 ± 115	1310 (1550) 1950	Sheridan River near site G. *In situ* stump buried in outwash beyond outermost moraine.	1
I-1692	230 ± 110[e]	1470 (1700) 1950	Sheridan River near site G. *In situ* stump buried in outwash beyond outermost moraine.	1
β-98,986	230 ± 60	1490 (1730) 1950	Site F. Outer rings of stump, crossdated age span of stump A.D. 1360–1512.	2
Sherman Glacier				
CURL-5297	1180 ± 40	720 (840) 970	Near site N. Single growth ring from *in situ* stump under boulder, first and last ring dates are 833 and 1002 ± 125 cal. A.D. at 2σ range.	2
Saddlebag Glacier				
β-93,992	260 ± 50	1480 (1640) 1950	Site P. Outer rings of *in situ* stump, crossdated age span of stump A.D. 1486–1615.	2

[a] Laboratories: β-, Beta Analytic, I-, Teledyne Isotopes Inc., CURL-, University of Colorado at Boulder.
[b] β- and CURL-ages are corrected for fractionation using measured $\delta^{13}C$.
[c] Median age in parentheses together with maximum and minimum ages of 2σ range. B.C. ages are negative.
[d] Sources: 1 – Tuthill et al. (1968), 2 – this study.
[e] Assumed 1σ range.

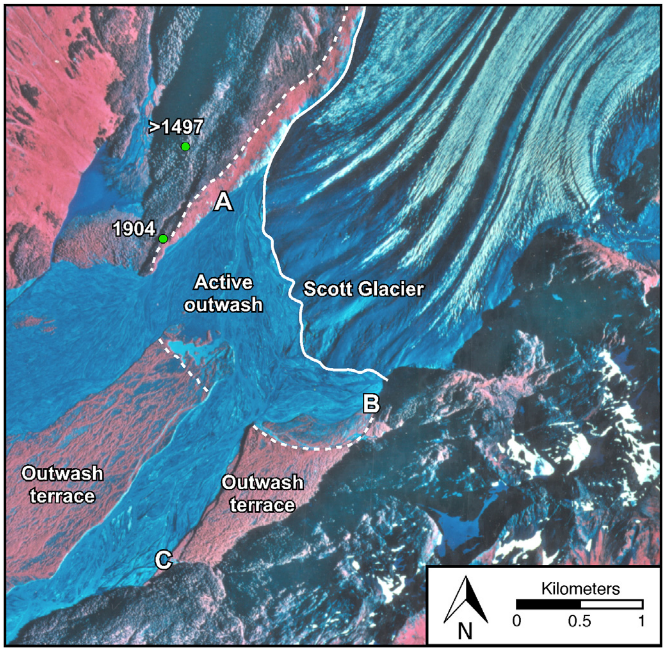

Fig. 4. Scott Glacier forefield. Solid line is 1996 ice margin, dashed line marks Little Ice Age maximum, green dots are dates of land surface stabilization, and letters A to C are subfossil wood sample sites. False-color photograph taken July 16, 1996. (For interpretation of the references to color in this figure legend, the reader is referred to the web version of this article.)

construction of the outermost Holocene moraine ridge on the southern side of the forefield (Fig. 6). Outwash also spread ahead of the ice margin during this interval to produce a largely continuous layer of sand and gravel across the lowland beyond the Holocene maximum position.

The oldest living trees found in the modern forest on the proximal outwash indicate land surface stabilization, at least locally, in 1600 (Fig. 5). A hemlock in a kettled area at the western edge of the forefield shows disturbed growth from the first ring in 1737— until 1769, suggesting stagnation of this area of the terminus with forest growth over dead ice. Farther south, trees indicate ice margin retreat and stabilization of the outermost moraine ridge in 1746 and a recessional moraine in 1777. This retreat was interrupted by a major re-advance in the 19th century. Trees that had germinated by 1705 on outwash at site G were killed by localized outwash aggradation in the 1850s (Fig. 6), and the rotted boles of some of these *in situ* stumps still protrude through the modern land surface today.

The large moraine at the southwestern shore of the current proglacial lake marks the culmination of the 19th century re-advance, and living trees show that the outer edge of this moraine was becoming ice free in 1874 (Fig. 5). Thinning and retreat continued into the 20th century (Tarr and Martin, 1914) and by the 1930s the southwestern and southern edges of the Sheridan terminal lobe were withdrawing from the inner edge of the large moraine into the lake basins (Tuthill et al., 1968; Field, 1975). Aerial photographs show multiple lakes feeding separate outlet rivers around the ice margin in 1950, and through the 1960s to 1980s

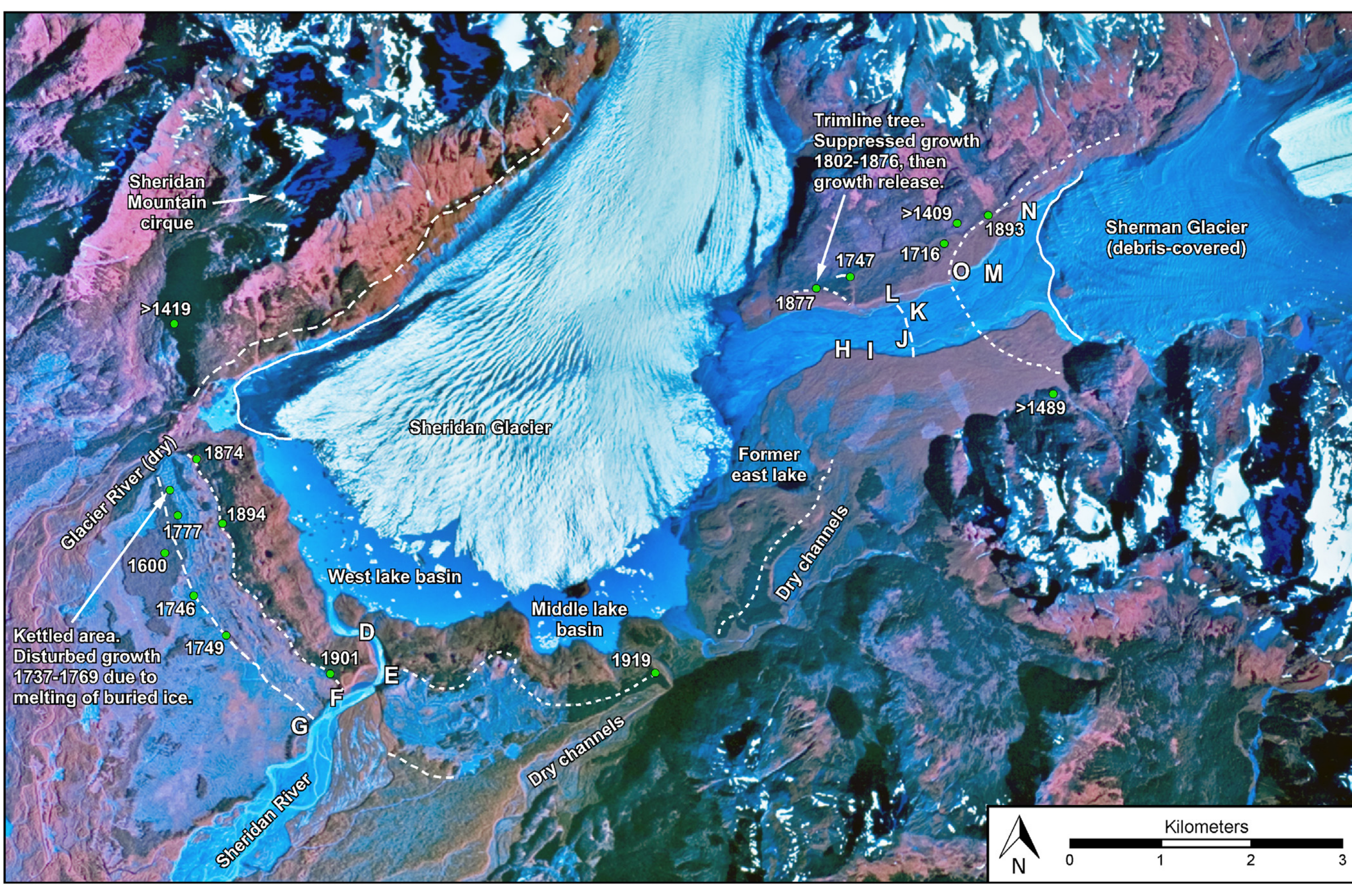

Fig. 5. Sheridan and Sherman glacier forefields. Solid lines are 1996 ice margins, dashed and dotted lines mark Little Ice Age maxima, green dots are dates of land surface stabilization, and letters D to O are subfossil wood sample sites. False-color photograph taken July 16, 1996. (For interpretation of the references to color in this figure legend, the reader is referred to the web version of this article.)

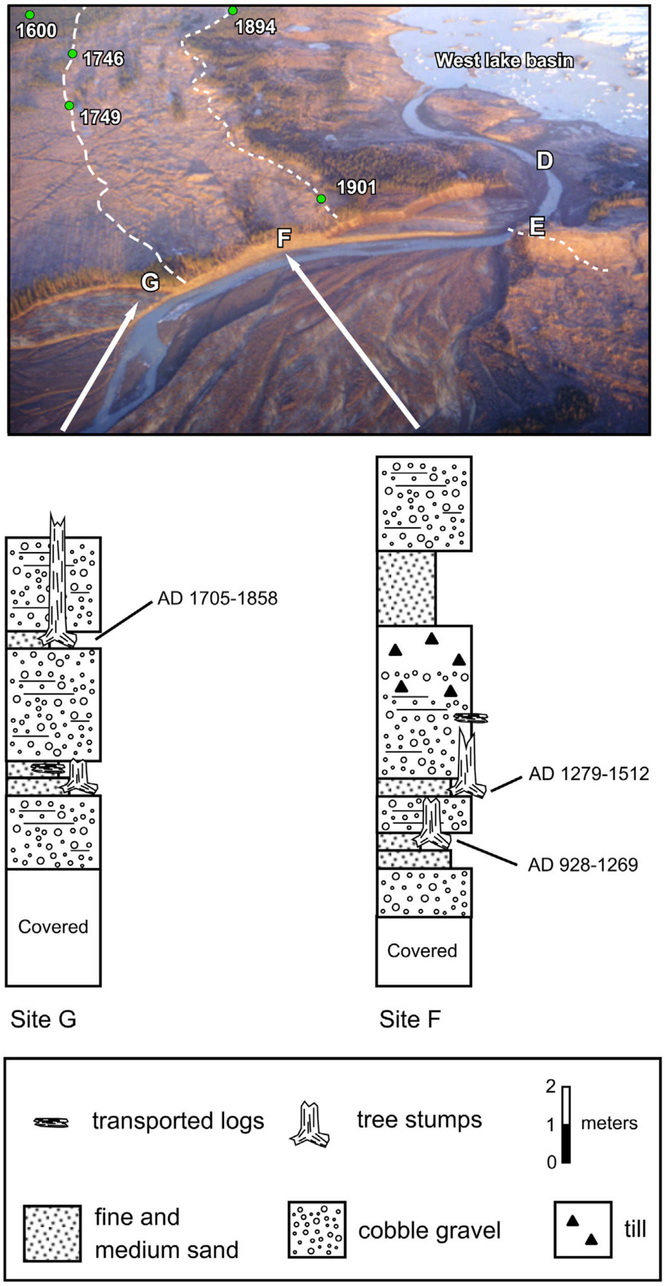

Fig. 6. Stratigraphy and geomorphology of western Sheridan forefield. Photo by P.J. Fleisher, January 1994.

these lakes coalesced with ultimately all drainage focused into the west basin and thence into Sheridan River. Erosion of this lake outflow threshold progressively lowered water level in the west basin by meters since 1950, and maximum water depths near the ice margin in the west lake basin were measured at over 125 m in 1999 (P.J. Fleisher, personal communication, 1999).

In 1950 the southwestern Sheridan ice margin was about 1500 m from the *c*.1746 position, and a further 800 m of retreat occurred in the west lake basin by 2000. In contrast, the margin at the island in the middle lake basin only retreated about 100 m between 1950 and 1978, and showed almost no further change to 2000. Retreat has also been minimal since 1950 at the western edge of the terminus where surficial debris covers the ice (Fig. 5). Thinning of the terminus has led to fragmentation and collapse of the eastern edge of the lobe; large icebergs and areas of brash ice are evident near the former east lake basin in 1996 photographs (Fig. 5) and Landsat images show ~1.5 km^2 of fragmentation between 2000 and 2009.

3.4. Sheridan Glacier – eastern forefield

Late Holocene fluctuations of Sheridan Glacier are also recorded in the eastern forefield (Fig. 5). This side of the Sheridan terminus controls base level in the west-draining valley that leads from Sherman Glacier, and incision by Sherman meltwater and meteoric streams has exposed valley fill deposits at the sides and floor of the valley. Lateral and end moraines of Sheridan Glacier are preserved at the northwestern edge of the valley.

A till unit at site H contains logs that were collectively alive from 334 to 577, and the clustering of last years of growth in the 560s and 570s (Fig. 3) suggests that at this time these trees were killed and moved eastwards by the expanding Sheridan terminus. This till unit is laterally continuous to site I (Fig. 5), where the till becomes interbedded with outwash, and then farther east the unit is just outwash and contains one log crossdated at 318 to 536. We interpret site I to be the eastern limit of this First Millennium A.D. advance and this is about 600 m short of the late Holocene maximum of Sheridan Glacier.

The First Millennium A.D. deposits at sites H and I are exposed in a bluff about 15 m above the adjacent valley floor. This is higher in elevation than younger deposits exposed in the valley floor (described next), which indicates that the younger deposits are inset within rather than stratigraphically above the older deposits. Therefore, the Sheridan ice margin must have withdrawn far enough after the First Millennium A.D. advance to lower base level and allow the Sherman meltwater river to erode a sizable valley through the First Millennium A.D. deposits.

A total of 34 logs from sites J, K and L have been crossdated and collectively these trees were alive from 1253 to 1671 (Fig. 3), with last years of growth clustering in the 1650s and 1660s. Site J is in the current valley floor with the logs in till and outwash, site K is also in the valley floor with the logs in glacilacustrine clays, silts, and sands, and site L is an outwash deposit near to and about 3 m above site K (Fig. 5). The glacilacustrine unit at site K overlies an oxidized horizon developed in the top of an underlying outwash unit (Fig. 2f) with a soil organic layer at the contact. From these deposits we infer that this area was a sparsely vegetated outwash surface after erosion of the valley through the First Millennium A.D. deposits. The eastern edge of Sheridan Glacier reached into this area during the 1650s and 1660s with a shallow lake ahead of the advancing ice margin; logs were transported from terraces or the valley sides into the shallow lake (site K) or overrun by the ice margin (site J). Outwash from both Sheridan and Sherman glaciers then aggraded across the area and incorporated more logs (site L).

The late Holocene maximum of Sheridan Glacier in the eastern forefield is marked by the eastern limit of till in the valley floor at site J and a band of large boulders across the valley. High terraces along both the north and south sides of the valley show that outwash and other glacigenic deposits aggraded to 25–50 m above the current valley floor, with the final land surface sloping about 2% towards the west-southwest. Drainage from Sherman Glacier and the eastern Sheridan terminus during this maximum was diverted to channels between the southeastern edge of Sheridan and the adjacent mountainside (Fig. 5), and this meltwater either eroded away or prevented formation of end moraines in this channeled area around the outer edge of the Sheridan forefield.

The oldest living tree found on outwash terraces of the eastern Sheridan forefield indicates local stabilization of this land surface by 1716 (Fig. 5). Living trees on moraines at the northwestern edge of the valley show that Sheridan Glacier retreated from its outermost end moraine in 1747 and from a prominent lateral moraine ridge (Fig. 2b) in 1877. A spruce tree immediately beyond this latter moraine had an innermost ring date of 1802, increasingly suppressed growth until 1876, and then much better growth for the next 15 years; this is consistent with the Sheridan ice margin re-advancing to this position during the 1850s and beginning to retreat in 1877. Aerial photographs show that the channels around the southeastern edge of the Sheridan margin were progressively abandoned from the 1950s to 1970s, and that small lakes formed and disappeared during this same interval at the eastern edge of the Sheridan lobe. The outwash stream from Sherman Glacier has progressively incised through the valley fill deposits with sediment and excavated logs being transported west into the ice marginal drainage system of Sheridan.

3.5. Sherman Glacier

Sherman Glacier is located at the head of a large valley that drains west-southwest towards Sheridan Glacier (Fig. 5). Lateral moraines mark the late Holocene maximum on the north side of the valley, while deflected stream channels, kettles, and a lag of large boulders show the former ice limit on the alder-covered outwash terraces and across the valley center. Erosion by the Sherman meltwater river and valley side meteoric streams has exposed sediments and subfossil logs in the valley floor and adjacent terraces.

The oldest organic material found on the Sherman Glacier forefield was a hemlock stump about 100 m south of site N (Fig. 5). Although tree-ring samples did not crossdate with the master chronology, a single ring returned a radiocarbon age of 840 cal. yr. A.D. (CURL-5297, Table 3) that when considered with ring counts yields estimated first and last years of growth for the stump of 833 and 1002 $\pm$ 125 cal. A.D. at the 95% confidence level. The stump was deeply buried in outwash beneath a large boulder with the outer rings lost to abrasion, but it appears that forest was established here at the same time as trees were growing on the Sheridan forefield at sites E and F and at Glacier River.

Four tree-ring samples from site M (Fig. 5) did crossdate and record growth from at least 1360 to 1608 (Fig. 3). All four of these were badly abraded, two were *in situ* stumps, and these are probably of the same cohort as a number of unreachable *in situ* stumps nearby in the active Sherman Glacier meltwater channel. Collectively these samples record an interval of forest growth in the central valley with the trees killed by outwash from Sherman Glacier; some trees killed in this area may have been transported to and deposited as logs in the shallow lake dammed at site K.

Much better preserved *in situ* stumps were found at site N (Fig. 5). An older cohort of five stumps record growth from 1512 and were rooted on a sloping till and bedrock surface (Fig. 2d), while a younger cohort of five stumps have inner rings dating to the 1720s with roots too deeply buried to examine. All ten of these stumps had outer ring dates between 1815 and 1820 with six having bark or a pristine outer surface, and all were buried in outwash and till. Farther west, a transported log at site O was alive from 1761 to 1839 and was buried in outwash near the top of the main terrace. Collectively these data show that Sherman Glacier was up-valley of site N from at least 1512 to 1820, and suggest that a pulse of outwash may have provided a fresh substrate for tree germination in the 1720s. The Sherman ice margin was advancing to its late Holocene maximum in the 1810s through 1830s, and living trees beyond the late Holocene maximum show that this position has not been exceeded since at least 1409 (Fig. 5).

Living trees on an end moraine at the north side of the valley indicate retreat of Sherman Glacier was underway in 1893 (Fig. 5) and by 1964 the ice margin was 1200 m behind this maximum position (Field, 1975). However, a large volume rock avalanche fell onto the terminus during the 1964 earthquake (Shreve, 1966) and by 1971 this debris was reaching the ice margin. Aerial photographs and Landsat images show that by 1978 the terminus was re-advancing, and in 2000 the ice margin had substantially thickened and was 950 m from the *c*.1893 position.

3.6. Saddlebag Glacier

Saddlebag Glacier occupies a narrow valley immediately west of the mouth of the Copper River and currently terminates in a deep proglacial lake (Fig. 7). Several end moraines rim the south shore of this lake and outwash deposits extend toward the Copper River Delta. Although spruce trees grow at the southern end of this valley, alder dominates the northern areas around the lake and on the adjacent mountain slopes.

The oldest organic materials found were six *in situ* spruce and cottonwood stumps in the outlet river at site P (Fig. 7). Two of the spruce samples crossdated and together record growth from 1486 to 1636. Although the sediments in which these stumps were buried have been swept away, we infer by the intactness of the stumps that they were buried in outwash before the ice margin overran the growth site. An end moraine on the west side of the valley likely marks the limit of this advance (Fig. 7), but we were unable to visit it and so this maximum remains undated.

The oldest spruce trees growing on outwash farther south show local land surface stabilization by 1645 (Fig. 7). A large moraine just north of site P lacks old spruce, but a core from a cottonwood indicates ice retreat in 1897. This is consistent with an 1899 photograph of Saddlebag Glacier by H.P. Ritter that shows a narrow barren zone at the ice margin, no lake, and outwash extending southwards (Tarr and Martin, 1914). Aerial photographs show the terminus formed a narrow tongue occupying much of the lake

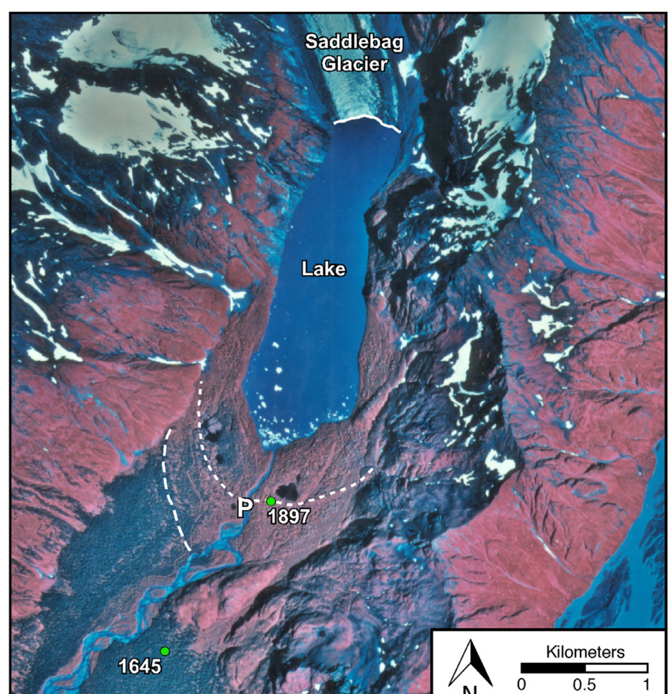

Fig. 7. Saddlebag Glacier forefield. Solid line is 1996 ice margin, dashed and dotted lines mark Little Ice Age maxima, green dots are dates of land surface stabilization, and letter P is a subfossil wood sample site. False-color photograph taken July 16, 1996. (For interpretation of the references to color in this figure legend, the reader is referred to the web version of this article.)

basin in the 1940s and 1950s; this tongue fragmented in 1959 or 1960 (Field, 1975) and in 1976 the ice margin was a steep iceberg-calving cliff 3050 m from the outermost moraine. The margin stayed around this same position until at least 1985, significant additional retreat had occurred by 1996, and in 2000 the margin was 3600 m from the outermost moraine.

4. Discussion

4.1. Synthesis of forefield records

Integration of the dates and locations of crossdated wood with glacial stratigraphy and geomorphology (Fig. 8) shows four distinct intervals of advance in the past two millennia. The first two advances, from the 530s to *c.*640s in the First Millennium A.D. (FMA) and 1240s to 1280s in the early Little Ice Age (LIA), are only recorded on the Sheridan forefield and are separated by a lull in glacial activity from *c.*800s to 1200s during the Medieval Warm Period (MWP). Both Sheridan and Saddlebag glaciers advanced between the 1510s and 1700s during the middle LIA, reached their Holocene maxima, and subsequently retreated. Scott and Sherman glaciers may also have advanced during this time, as indicated by distinct cohorts of trees that began growing in the 1710s and 1720s on presumably middle LIA outwash deposits. All four termini show a strong advance in the 1810s to 1860s during the late LIA with subsequent retreat beginning in the 1870s to 1900s; this late LIA

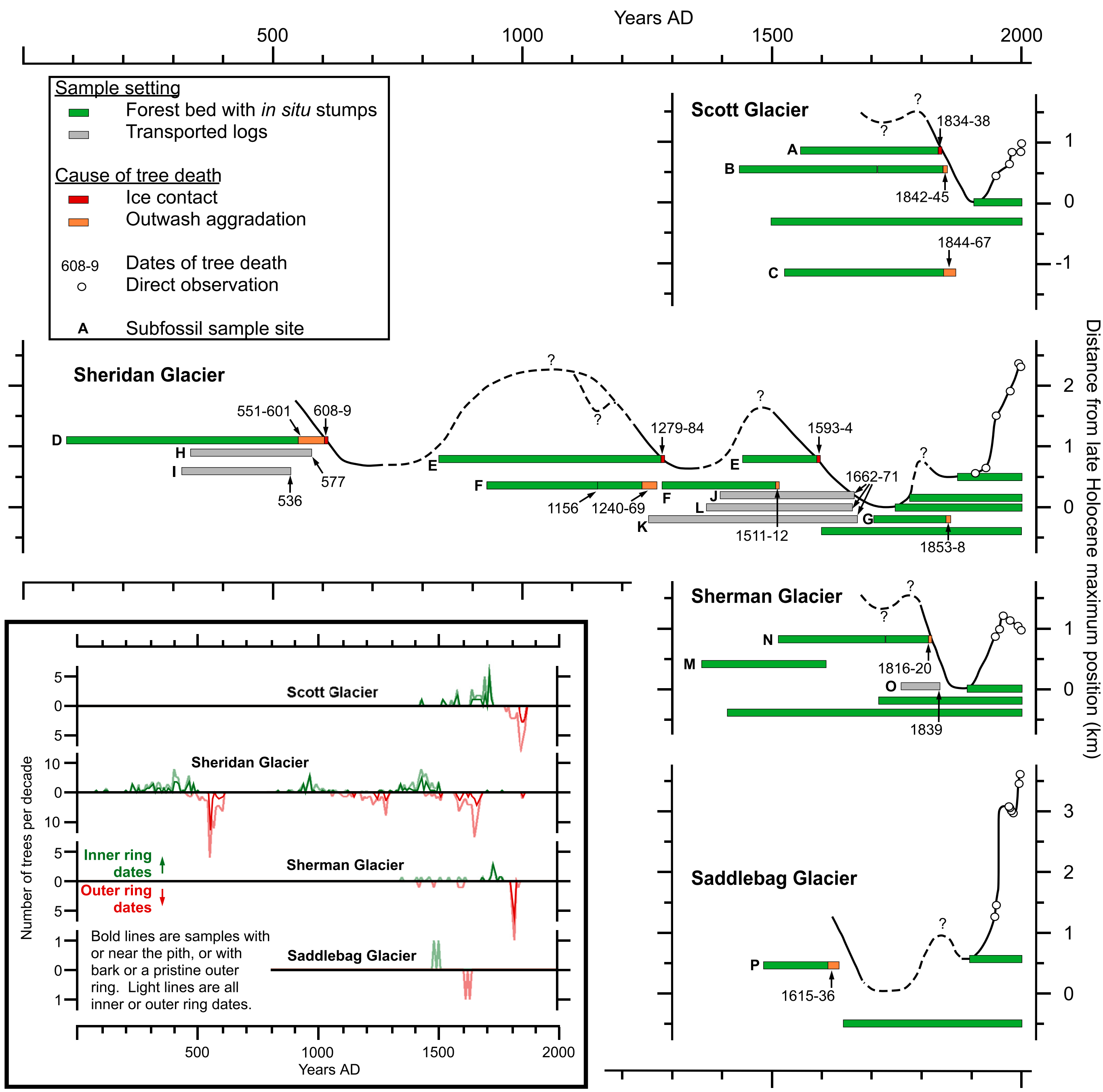

Fig. 8. Time-distance diagrams for study glaciers. Horizontal blocks show intervals of forest growth on and around forefields, and dashed and solid curves show inferred terminus positions. Inset summarizes inner and outer ring dates from samples in Fig. 3 ($n = 216$).

advance was the Holocene maximum for both Scott and Sherman glaciers.

The record from Sheridan Glacier is exceptional in terms of length, detail, and dating control. Although a number of other forefields in southern Alaska have fragmentary evidence of these same four intervals of advance (Wiles and Calkin, 1994; Wiles et al., 1999; Reyes et al., 2006; Barclay et al., 2009b), only the record of Tebenkof Glacier (Barclay et al., 2009a) comes close to the length and completeness of the Sheridan Glacier record. The Sheridan forefield is the first site in the region with calendar tree-ring crossdates for trees killed by all four major advances of the last two millennia. Furthermore, it is the only site found thus far where the limits of the FMA and early LIA advances are spatially constrained, with both being about 600 m short of the late Holocene maximum.

A potential concern is that only 53 (25%) of the 216 logs and stumps crossdated in this study had bark or a pristine outermost ring (Fig. 3). However, comparison of these best dates for tree death with last-ring dates for all available samples (Fig. 8 insert) shows close correspondence, with many other samples seemingly having lost just a few of their outer rings. Inner ring dates from the FMA forest bed at Sheridan Glacier (Fig. 8 insert) have a wide temporal spread, supporting our interpretation that this was an old growth forest in which tree recruitment was steady and ongoing. Inner ring dates from LIA forest beds are more clustered, consistent with the availability of fresh substrates creating distinct germination cohorts, but these dates are still more spread-out than the well-clustered dates of forefield tree death.

We used a 10-year ecesis estimate for conifers in this study, which is shorter than the 15- to 25-year ecesis times used at most other sites in coastal south-central Alaska (Vierek, 1967; Wiles and Calkin, 1994; Crossen, 1997; Wiles et al., 1999). Nonetheless, this 10-year ecesis is supported by the concordance of the 1877 moraine age calculated with this estimate at the eastern Sheridan forefield and the post-1876 growth release in an adjacent trimline tree. Also, trees at site F on the southern Sheridan forefield were growing again by 1279 following outwash aggradation from 1240 to 1269 (Fig. 6). Rapid germination of trees on new substrates on these Copper River Delta forefields may be favored by their near coastal setting, with onshore winds helping move the seeds of these conifers towards the glaciers and moderating temperatures year-round.

4.2. Outwash aggradation and incision

The tree-ring and glacial geologic data show a general association of outwash aggradation with intervals of ice margin advance, with trees killed by both outwash deposition and direct contact with ice margins during the late LIA at Scott Glacier, and during the FMA, early LIA, and middle LIA advances on the southern Sheridan forefield (Fig. 8). However, exact dates for outwash aggradation vary from being before (e.g. site F) to after (e.g. site B) nearby dates of tree death from ice contact. Outwash deposition was also spatially variable. It occurred in the 1840s to 1860s at site C, which at the time was at least two kilometers ahead of the advancing Scott ice margin, but had ceased at site F by 1279 enabling trees to germinate, even though the nearby Sheridan ice margin was still advancing until at least 1284 at site E (Figs. 6 and 8).

We infer that during times of sustained terminus advance, outwash aggradation generally occurred along one or more discrete linear zones on each forefield with areas of undisturbed forest and inactive outwash in-between (Fig. 9a). Each active outwash corridor was the axis of a river system fed by a meltwater portal in the ice margin, and these channels migrated across the forefields to ultimately deposit sheets of outwash. Death dates for trees killed by outwash aggradation often spanned decades at a site (Fig. 8), reflecting the progressive encroachment of meltwater into forest. In contrast, trees growing on old moraines, valley sides, and bedrock knobs were above the general level of outwash aggradation and so could only be killed as the ice margin over-ran the growth site, causing death dates to be clustered into just a few years. Trees were able to begin recolonizing inactive outwash almost as soon as deposition ceased, regardless of whether the nearby ice margin was advancing or not.

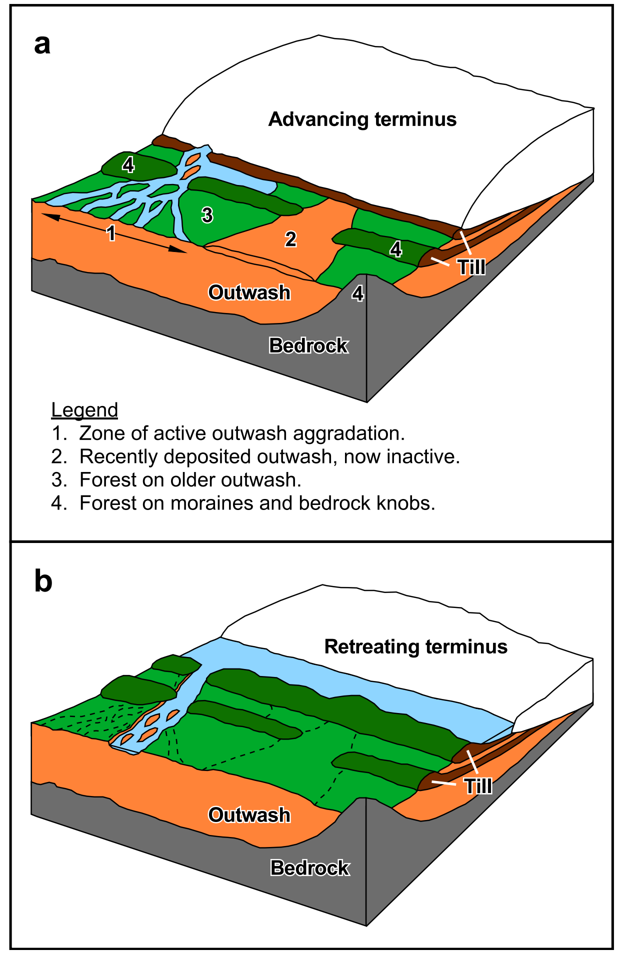

Fig. 9. Block diagrams of forefield geomorphology and forest cover during terminus advance and retreat. (a) During advance, outwash aggrades along the axis of active meltwater streams and encroaches into forest growing on older outwash. Trees can recolonize inactive outwash surfaces, even though the nearby ice margin is advancing. Trees on old moraines and elevated bedrock sites can only be killed if the ice margin advances to the growth site. (b) During retreat the meltwater river incises, and trees across the forefield and proximal outwash area are relatively undisturbed by glacifluvial processes.

Meltwater rivers of the study glaciers have incised through forefields and proximal outwash areas during 20th and 21st century termini retreat (Figs. 4–7). As a result, outwash cannot aggrade on the now elevated outwash surfaces and so forest growth is relatively undisturbed by glacifluvial processes (Fig. 9b). Meltwater impacts on forefield forests are currently limited to undercutting of terrace margins during lateral channel migration and occasional channel avulsions. Presumably this current situation is similar to previous periods of terminus retreat, when growth of forefield forests also appear to have been mostly undisturbed by outwash.

A sediment core from Cabin Lake (Fig. 1) provides additional insight into development of the western edge of the distal outwash plain of Sheridan Glacier. Glacial silt is absent from the core through the middle to late Holocene, is present for most of the 1110–

1780 cal. A.D. interval, and then is absent again in the most recent sediments at the core top (Zander et al., 2013). This record may reflect the inlet entrance to the Cabin Lake basin being higher than the adjacent Sheridan outwash surface during the middle to late Holocene, thus keeping this small basin isolated from Sheridan meltwater. Late Holocene aggradation of the distal outwash plain may have been responsible for directing meltwater into the basin during the last millennium, and incision by the nearby Glacier River (Fig. 5) after the middle LIA maximum of Sheridan Glacier may have prevented meltwater from returning to Cabin Lake during the late LIA. The onset of silt deposition at about 1110 cal. A.D. (Zander et al., 2013) may also support the inference of a small advance of Sheridan Glacier and brief interval of outwash aggradation at this time (Fig. 8), which otherwise is based on just a single crossdated tree-ring sample from site F.

4.3. Climatic forcing of valley glacier fluctuations

Globally the only tree-ring constrained valley glacier histories with length and detail comparable to the Sheridan Glacier record are those of Great Aletsch and Gorner glaciers in Switzerland (Holzhauser et al., 2005) and Tebenkof Glacier in south-central Alaska (Barclay et al., 2009a). Comparison shows strong agreement (Fig. 10), with all four termini having made large advances in

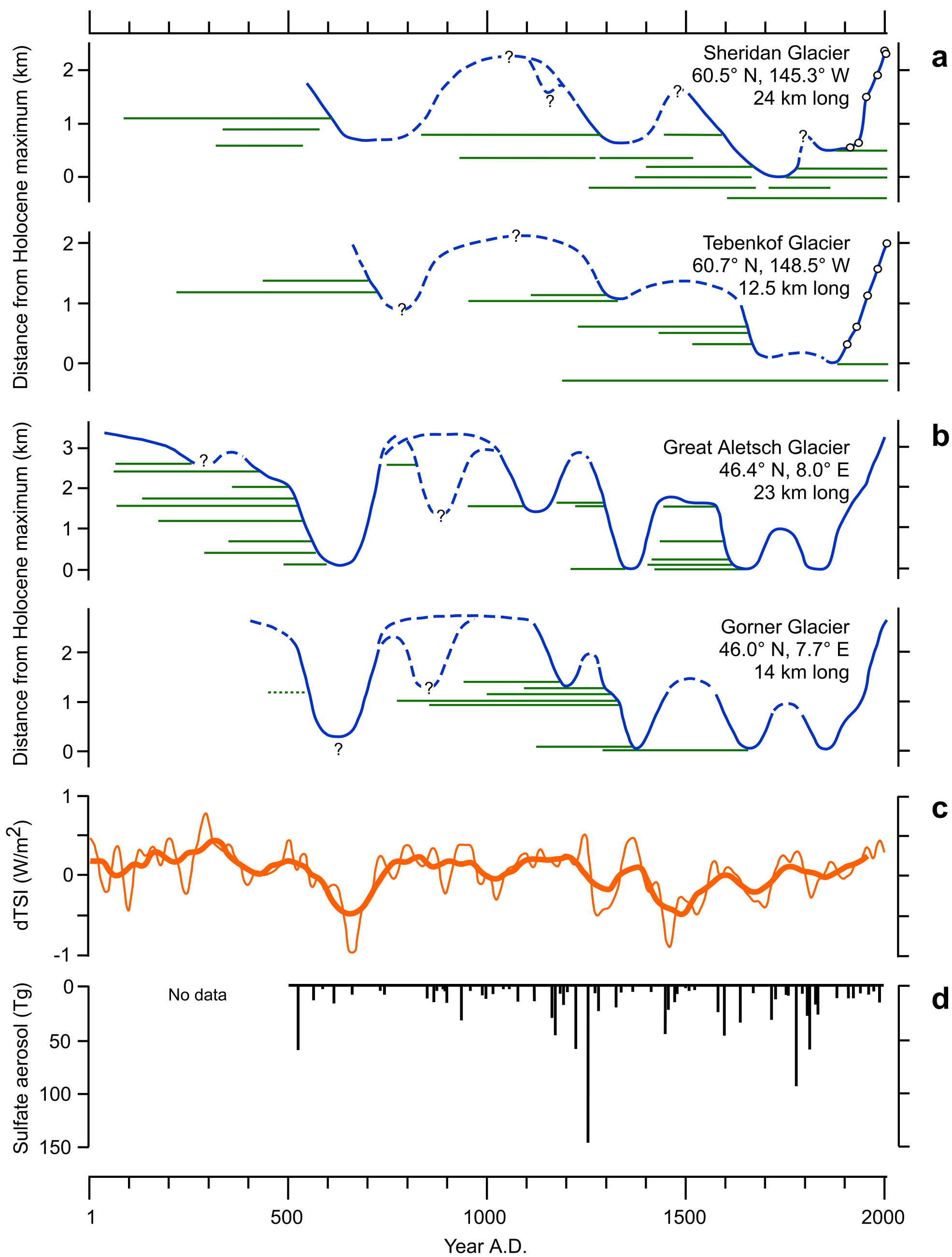

Fig. 10. Tree-ring dated late Holocene valley glacier fluctuations and global and hemispheric forcing factors. (a) Time-distance diagrams for two glaciers in coastal south-central Alaska. Horizontal bars are periods of forefield forest growth based on tree-ring crossdates, circles are direct observations of ice margins, and solid and dashed curves are inferred terminus positions. Tebenkof record updated from Barclay et al. (2009a). (b) Time-distance diagrams for two valley glaciers in Switzerland. Dotted horizontal bar based on a radiocarbon age, other symbols as in panel a. From Holzhauser et al. (2005). (c) Total solar irradiance reconstructed using ^{10}Be in ice cores. Bold line is 100-year running average. From Steinhilber et al. (2009). (d) Northern hemisphere volcanic sulfate aerosols based on ice cores. From Gao et al. (2008).

the FMA and then three distinct advances during the LIA. The MWP is also apparent on all four forefields with termini significantly retracted from their extents during the FMA and LIA periods. There are some differences: the FMA and early LIA advances of Sheridan and Tebenkof glaciers were less extensive than the corresponding advances of Great Aletsch and Gorner glaciers, and there is variability with the exact decades when advances, maxima, and retreats occurred. Nonetheless, the overall coherence of these mid-latitude valley glacier histories suggests that these fluctuations reflect a common global or hemispheric climatic forcing.

Total solar irradiance (TSI) is one possible climatic forcing factor and these intervals of glacier advance (Fig. 10) coincide with decreases of TSI in the reconstruction by Steinhilber et al. (2009). The FMA ice advances occurred at or soon after a large TSI drop from *c*.500 to 700, and the LIA advances were during a sustained period of generally below average TSI from 1200 to 1900. The dates of the middle and late LIA maxima also show close correspondence with century scale drops in TSI. Coherence of solar irradiance and glacier fluctuations has previously been demonstrated statistically for termini in both Alaska (Wiles et al., 2004) and the Swiss Alps (Hormes et al., 2006). These temporal linkages are also supported by multiple physical mechanisms by which TSI can affect glaciers, such as the direct effects on ice ablation of insolation and air temperature (Kuhn, 1979). Changes in regional temperature also affect the freezing level height, which controls the proportion of precipitation that falls as snow versus rain, and so will affect glaciers via both snow accumulation and rain-induced melting (Meier, 1965; Arendt et al., 2009).

Explosive volcanic eruptions that inject sulfate aerosols into the stratosphere are another potential global to hemispheric forcing factor for valley glacier fluctuations (Porter, 1986; Robock, 2000). Such aerosols block insolation and cause surface cooling for a few years after an eruption, but comparison of the Northern Hemisphere sulfate aerosol reconstruction of Gao et al. (2008) with the valley glacier record shows less correspondence than TSI forcing (Fig. 10). Miller et al. (2012) suggest that feedbacks from sea ice formation in the North Atlantic were sufficient to sustain cooling from five eruptions between 1228 and 1285, and that this was a major factor in the onset of the LIA. However, the early LIA advance of Sheridan Glacier was underway before all but one of these eruptions, as were advances of Princeton and Billings glaciers in western Prince William Sound (Wiles et al., 1999) and Robson Glacier in the Canadian Rockies (Luckman, 1995), meaning that volcanic effects alone cannot have forced these mid-latitude glacier advances.

A complication with both solar and volcanic forcing is that these drivers also affect the Earth's latitudinal temperature gradient, which controls the vigor of atmospheric circulation, and the resulting changes in surface air mass movement can offset or even reverse the direct radiative effects on local temperature (Lough and Fritts, 1987; Robock, 2000; Davis and Brewer, 2011). Changes in air mass movement can also have hydrological effects that significantly influence glacier mass balances (Nesje and Dahl, 2003; Vincent et al., 2005; Magny et al., 2010), and changes to coupled atmospheric–oceanic systems from either internal variability or external forcing can also potentially affect glacier behavior (Bond et al., 2001; Denton and Broecker, 2008; Licciardi et al., 2009; Schaefer et al., 2009; Putnam et al., 2012; Lowell et al., 2013). These factors may explain some of the decadal-scale differences between the glacier histories from Switzerland and Alaska. Nonetheless, the overall correspondence of the TSI record with these glacier records suggests that solar irradiance has been the primary pacemaker for centennial-scale fluctuations of these mid-latitude valley glaciers.

4.4. Localized glacier-specific controls

One clear difference between the records of Copper River Delta glaciers is with the magnitude of the middle and late LIA advances (Fig. 8). Although all four termini made both advances, the middle LIA advance was larger at Sheridan and Saddlebag while the late LIA advance was larger at Scott and Sherman. The proximity of these four termini means that this difference in magnitude of advance cannot have a direct climatic cause. This situation also occurs throughout coastal south-central Alaska, with adjacent termini often differing with exactly when in the LIA the late Holocene terminal moraine formed (Fig. 11). These differences in magnitude of advance likely reflect local factors such as glacier geometry, hypsometry, slope, or orientation that can affect the specific response of glaciers to climatic forcing (e.g. Pelto and Hedlund, 2001).

Bull and Maranguanic (1968) suggested that debris from the 1964 co-seismic rock avalanche onto Sherman Glacier would reduce ablation on the lower glacier and cause a re-advance and this has indeed happened, albeit less dramatically than predicted (Bull, 1969). Debris cover is also likely the reason for the stagnation of the western margin of Sheridan Glacier (Fig. 5) at the *c*.1740 maximum and the lower retreat rate of this side of the terminus in the 20th century, and may also partially explain the relatively small 20th century retreat of Scott Glacier (Fig. 4). The overall coherence of these glacier histories, however, suggests that effects from surficial debris have not substantially altered these glacier histories and that co-seismic rock avalanches large enough to force re-advances are rare.

Lacustrine iceberg-calving termini generally retreat farther and faster than land-based termini (Wiles and Calkin, 1994; Boyce et al., 2007), and this is evident in the 20th century records of Sheridan and Saddlebag glaciers. However, these glaciers did not develop proglacial lakes and iceberg-calving termini until significant retreat had already occurred, both had terrestrial termini during their LIA maxima, and the spread of outwash across the southern Sheridan forefield suggests that Sheridan Glacier may have been a terrestrial ice margin through most of the past two millennia. These proglacial lake basins may be very recent features of the forefields, reflecting excavation of subglacial overdeepenings during the LIA maxima, and so have not substantially altered the timing of termini fluctuations.

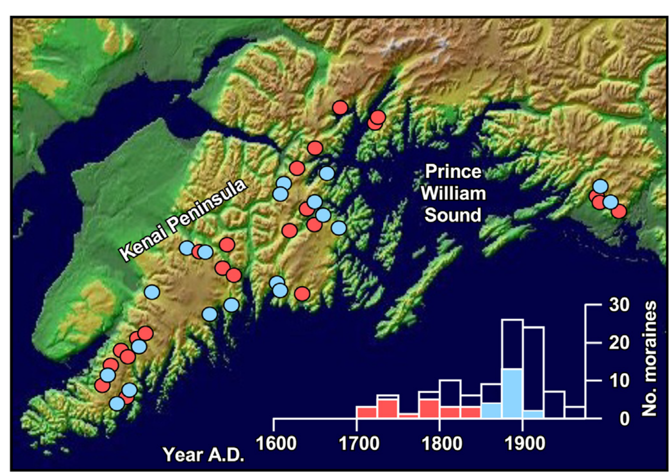

Fig. 11. Late Holocene moraine dates in coastal south-central Alaska. 1751–1850 terminal moraines in red ($n = 23$), 1851–1925 terminal moraines in blue ($n = 19$), and recessional moraines as hollow bars. Updated from Barclay et al. (2009b), dataset in Table A1. (For interpretation of the references to color in this figure legend, the reader is referred to the web version of this article.)

5. Conclusions

(1) Valley glacier histories have been reconstructed for four termini on the Copper River Delta in coastal south-central Alaska. The combined use of tree-ring crossdates of glacially killed trees, living tree ages, glacial stratigraphy and geomorphology, and historical photographs and observations provides high temporal and spatial resolution to these records.

(2) Sheridan Glacier has made four major advances during the past two millennia: from the 530s to *c*.640s in the First Millennium A.D. (FMA), and from the 1240s to 1280s, 1510s to 1700s and *c*.1810s to 1860s during the Little Ice Age (LIA). The greatest extent was attained between *c*.1700s and 1740s, and the other three advances culminated about 500–600 m short of the Holocene maximum.

(3) Nearby termini of Scott, Sherman, and Saddlebag glaciers have less complete forefield records and show evidence of just the last two phases of advance seen at Sheridan. The timing of these middle to late LIA advances was the same for all four termini, but the magnitude of advances differed.

(4) The record of Sheridan Glacier is very similar to the two-millennia-long tree-ring constrained records of Tebenkof Glacier in south-central Alaska and Great Aletsch and Gorner glaciers in Switzerland. Coeval advances of these termini correspond with decreases in solar irradiance, supporting output from the Sun as the primary pacemaker for centennial-scale fluctuations of these mid-latitude valley glaciers prior to the 20th century.

(5) Volcanic aerosols and coupled atmospheric-oceanic systems may have played a supplemental role in forcing fluctuations and in causing decadal-scale differences in the histories. Local glacier-specific factors likely affect the magnitude of glacier response to climatic forcing, but do not appear to have substantially affected the timing of major advances over the past two millennia.

Acknowledgments

This work was supported by the National Science Foundation under Grants 9912124 and 9905493. We thank Gordon Jacoby, Gregory Wiles, and Suzanne Lucas for assistance in the field, and Nancy Sullivan and Sarah Green for help with some of the tree-ring analyses. The Eyak Corporation granted permission to work on the southern Sheridan forefield, and the Prince William Sound Science Center and the Chugach National Forest – Cordova Ranger District provided some logistical support. Geospatial data were obtained from the Alaska Statewide Digital Mapping Initiative (http://browse.alaskamapped.org) and the Chugach National Forest GIS at the FSGeodata Clearinghouse (http://fsgeodata.fs.fed.us). Reviews by Darrell Kaufman and P. Thompson Davis led to improvements in the clarity of the paper.

Appendix

Table A1
Dates of moraine stabilization for valley and cirque glaciers in coastal south-central Alaska.

Glacier	Moraine dates[a]	Ecesis[b]	Sources[c]
Grewingk–Yalik ice complex			
Yalik	**1889**[L], 1900[L], 1909	15	3
Kristen cirque	**1799**[L], 1881[L]	–	3
Petrof	**1904**, 1915, 1939	15	3
Wosnesenski	**1828**, 1858, 1903[L], 1915[L]	15	3
Grewingk	**1858**, 1904[L], 1914[L], 1926[L]	15	3
Portlock	**1848**	15	3
Cyrus cirque	**1759**[L], 1903[L], 1921[L]	–	3
Nuka	**1724**, 1736, 1814, 1816, 1847, 1872, 1882, 1913, 1951	15	3
Harding Icefield			
Kachemak	**1879**[L], 1914[L], 1929[L]	–	3
Goat	**1799**[L], 1848[L], 1918[L]	–	3
Dinglestadt	**1824**, 1878, 1905	15	3
Tustemena	**1864**	15	3
Skilak	**1881**[L]	–	3
North Goat	**After 1660 cal. A.D.**, 1890[L]	–	8
North Goat cirque 2	**1890**[L]	–	8
North Goat cirque 12	**1820**[L], 1930[L]	–	8
Exit	**1825**, 1899, 1909, 1924, 1927, 1951	15	3
Marathon Mtn. cirque	**1750**[L], 1812[L], 1885[L]	–	6
Bear	**1888**, 1909	15	3
Pederson	**1885**, 1909, 1912, 1920, 1930, 1951	15	3
Sargent Icefield:			
Ellsworth	**1855**, 1918	15	5
3rd July	**1874**	15	5
Excelsior	**1797**, 1917	15	5
Ultramarine	**1889**	15	5
Falling	**1875–1885**	20	2
Langdon-Kings	**1737**, 1889	15	5
Spencer–Blackstone ice complex			
Wolverine	**1713**, 1777, 1807	15	5
Taylor	**1725**, 1893	15	5
Cotterell	**1891**	15	5
Tebenkof	**1891**, 1912	15	5, 7
Portage	**Before 1799**, 1810, 1859, 1900	25	4
Spencer	**1890s**	5–10	2
Bartlett	**1890s**	–	4

(*continued on next page*)

Table A1 (*continued*)

Glacier	Moraine dates[a]	Ecesis[b]	Sources[c]
Coastal Chugach Mountains:			
Billings	**1742**, 1818, 1850, 1894	15	5
Baker	**1785**, 1892	15	1
Crescent	**1780**, 1807, 1935	15	6
Amherst	**1830**	15	6
Scott	**1904**	10	9
Sheridan Mtn. cirque[d]	**1731**[L], 1874[L], 1908[L]	–	9
Sheridan	**1746**, 1777, 1874	10	9
Sherman	**1893**	10	9
Saddlebag	**After 1636**, 1897	10	9

[a] In years A.D. unless otherwise noted, Holocene terminal moraines in bold, lichen-based dates have [L] superscript.
[b] Ecesis estimate used for tree ring dates, in years.
[c] Sources: 1 – based on data in Tarr and Martin (1914), 2 – Vierek (1967), 3 – Wiles and Calkin (1994), 4 – Crossen (1997), 5 – Wiles et al. (1999), 6 – Wiles et al. (2008), 7 – Barclay et al. (2009a), 8 – Daigle and Kaufman (2009), 9 – this study.
[d] Located immediately west of Sheridan Glacier forefield (Fig. 5). Maximum diameters of lichen (*Rhizocarpon sensu lato*) measured in 1993 of 115 mm (outermost deposits), 47 mm (outer ridge crest) and 31 mm (inset ridge).

References

Abercrombie, W.R., 1900. Supplementary expedition into the Copper River Valley, Alaska. In: Compilation of Narratives of Explorations in Alaska. Government Printing Office, Washington, pp. 383–408.
Arendt, A., Walsh, J., Harrison, W., 2009. Changes of glaciers and climate in northwestern North America during the late twentieth century. J. Clim. 22, 4117–4134.
Barclay, D.J., Calkin, P.E., Wiles, G.C., 2001. Holocene history of Hubbard Glacier in Yakutat Bay and Russell Fiord, southern Alaska. Geol. Soc. Am. Bull. 113, 388–402.
Barclay, D.J., Wiles, G.C., Calkin, P.E., 2003. An 850 year record of climate and fluctuations of the tidewater-calving Nellie Juan Glacier, south central Alaska, U.S.A. Ann. Glaciol. 36, 51–56.
Barclay, D.J., Wiles, G.C., Calkin, P.E., 2009a. Tree-ring crossdates for a first millennium AD advance of Tebenkof Glacier, southern Alaska. Quat. Res. 71, 22–26. http://dx.doi.org/10.1016/j.yqres.2008.09.005.
Barclay, D.J., Wiles, G.C., Calkin, P.E., 2009b. Holocene glacier fluctuations in Alaska. Quat. Sci. Rev. 28, 2034–2048.
Boggs, K., 2000. Classification of Community Types, Successional Sequences, and Landscapes of the Copper River Delta, Alaska. U.S. Forest Service General Technical Report PNW-GTR-469, p. 244.
Bond, G., Kromer, B., Beer, J., Muscheler, R., Evans, M.N., Showers, W., Hoffman, S., Lotti-Bond, R., Hajdas, I., Bonani, G., 2001. Persistent solar influence on North Atlantic climate during the Holocene. Science 294, 2130–2136.
Boyce, E.S., Motyka, R.J., Truffer, M., 2007. Flotation and retreat of a lake-calving terminus, Mendenhall Glacier, southeast Alaska, USA. J. Glaciol. 53, 211–224.
Brooks, A.H., 1908. Reconnaissance map of Chitina Quadrangle, Copper River Region, Alaska. In: Moffit, F.H., Maddren, A.G. (Eds.), Mineral Resources of the Kotsina-chitina Region, Alaska, U.S. Geological Survey Bulletin, 374, 1909, 1 Plate.
Bull, C., 1969. The 1978–1980 surge of Sherman Glacier, south-central Alaska. Can. J. Earth Sci. 6, 841–843.
Bull, C., Maranguanic, C., 1968. Glaciological effects of debris slide on Sherman Glacier. In: The Great Alaska Earthquake of 1964 – Hydrology. National Academy of Sciences Publication 1603, pp. 309–317.
Chapin, T., 1913. The McKinley Lake District. In: U.S. Geological Survey Bulletin 542-C.
Crossen, K.J., 1997. Neoglacial Fluctuations of Terrestrial, Tidewater and Calving Lacustrine Glaciers, Blackstone-spencer Ice Complex, Kenai Mountains, Alaska (Ph.D. dissertation). University of Washington, 198 pp.
Daigle, T.A., Kaufman, D.S., 2009. Holocene climate inferred from glacier extent, lake sedimentation, and tree rings at Goat Lake, Kenai Mountains, Alaska. J. Quat. Sci. 24, 33–45. http://dx.doi.org/10.1002/jqs.1166.
Davis, P.T., Menounos, B., Osborn, G., 2009. Holocene and latest Pleistocene alpine glacier fluctuations: a global perspective. Quat. Sci. Rev. 28, 2021–2033.
Davis, B.A.S., Brewer, S., 2011. A unified approach to orbital, solar, and lunar forcing based on the Earth's latitudinal insolation/temperature gradient. Quat. Sci. Rev. 30, 1861–1874.
Denton, G.H., Karlén, W., 1973. Holocene climatic variations – their pattern and possible cause. Quat. Res. 3, 155–205.
Denton, G.H., Broecker, W.S., 2008. Wobbly ocean conveyor circulation during the Holocene? Quat. Sci. Rev. 27, 1939–1950.
Field, W.O., 1975. Mountain Glaciers of the Northern Hemisphere, vol. 2. Cold Regions Research and Engineering Laboratory, Hanover, New Hampshire, p. 932.
Gao, C., Robock, A., Ammann, C., 2008. Volcanic forcing of climate over the past 1500 years: an improved ice core-based index for climate models. J. Geophys. Res. 133, D23111. http://dx.doi.org/10.1029/2008JD010239.
Grant, U.S., Higgins, D.F., 1909. Copper Mining and Prospecting on Prince William Sound. In: U.S. Geological Survey Bulletin 379-C.
Hormes, A., Beer, J., Schlüchter, C., 2006. A geochronological approach to understanding the role of solar activity on Holocene glacier length variability in the Swiss Alps. Geogr. Ann. 88A, 281–294.
Helm, D.J., Allen, E.B., 1995. Vegetation chronosequence near Exit Glacier, Kenai Fjords National Park, Alaska, U.S.A. Arct. Alp. Res. 27, 246–257.
Hoadley, R.B., 1990. Identifying Wood: Accurate Results with Simple Tools. The Taunton Press, Newtown, Connecticut, p. 223.
Holmes, R.L., 1983. Computer-assisted quality control in tree-ring data and measurement. Tree-ring Bull. 43, 69–78.
Holzhauser, H., Magny, M., Zumbühl, H.J., 2005. Glacier and lake-level variations in west-central Europe over the last 3500 years. Holocene 15, 789–801.
Hutchinson, I., Crowell, A.L., 2007. Recurrence and extent of great earthquakes in southern Alaska during the late Holocene from an analysis of the radiocarbon record of land-level change and village abandonment. Radiocarbon 49, 1323–1385.
Jóhannesson, T., Raymond, C., Waddington, E., 1989. Time-scale for adjustment of glaciers to changes in mass balance. J. Glaciol. 35, 355–369.
Kirkbride, M.P., Winkler, S., 2012. Correlation of late Quaternary moraines: impact of climate variability, glacier response, and chronological resolution. Quat. Sci. Rev. 46, 1–29.
Kuhn, M., 1979. Climate and glaciers. In: Sea Level, Ice, and Climatic Change. International Association of Hydrological Sciences Publication 131, pp. 3–20.
Licciardi, J.M., Schaefer, J.M., Taggart, J.R., Lund, D.C., 2009. Holocene glacier fluctuations in the Peruvian Andes indicate northern climate linkages. Science 325, 1677–1679.
Lough, J.M., Fritts, H.C., 1987. An assessment of the possible effects of volcanic eruptions on North American climate using tree-ring data, 1602 to 1900 A.D. Clim. Change 10, 219–239.
Lowell, T.V., Hall, B.L., Kelly, M.A., Bennike, O., Lusas, A.R., Honsaker, W., Smith, C.A., Levy, L.B., Travis, S., Denton, G.H., 2013. Late Holocene expansion of Istorvet ice cap, Liverpool Land, east Greenland. Quat. Sci. Rev. 63, 128–140.
Luckman, B.H., 1995. Calendar-dated, early Little Ice Age glacier advance at Robson Glacier, British Columbia, Canada. Holocene 5, 149–159.
Lutz, H.J., 1930. Observations on the invasion of newly formed glacial moraines by trees. Ecology 11, 562–567.
Magny, M., Arnaud, F., Holzhauser, H., Chapron, E., Debret, M., Desmet, M., Leroux, A., Millet, L., Revel, M., Vannière, B., 2010. Solar and proxy-sensitivity imprints on paleohydrological records for the last millennium in west-central Europe. Quat. Res. 73, 173–179.
Meier, M.F., 1965. Glaciers and climate. In: Wright, H.E., Frey, D.G. (Eds.), The Quaternary of the United States. Princeton University Press, New Jersey, pp. 795–805.
Miller, G.H., Geirsdóttir, A., Zhong, Y., Larsen, D.J., Otto-Bliesner, B.L., Holland, M.M., Bailey, D.A., Refsnider, K.A., Lehman, S.J., Southon, J.R., Anderson, C., Björnsson, H., Thordarson, T., 2012. Abrupt onset of the Little Ice Age triggered by volcanism and sustained by sea-ice/ocean feedbacks. Geophys. Res. Lett. 39, L02708. http://dx.doi.org/10.1029/2011GL050168.
Nesje, A., Dahl, S.O., 2003. The Little Ice Age – only temperature? Holocene 13, 139–145.
Pelto, M.S., Hedlund, C., 2001. Terminus behavior and response time of North Cascade glaciers, Washington, U.S.A. J. Glaciol. 47, 497–506.
Plafker, G., 1969. Tectonics of the March 27, 1964 Alaska Earthquake. U.S. Geological Survey, p. 174. Professional Paper 543-I.
Plafker, G., 1990. Regional vertical tectonic displacement of shorelines in south-central Alaska during and between great earthquakes. Northwest Sci. 64, 250–258.
Porter, S.C., 1986. Pattern and forcing of northern hemisphere glacier variations during the last millennium. Quat. Res. 26, 27–48.
Putnam, A.E., Schaefer, J.M., Denton, G.H., Barrell, D.J.A., Finkel, R.C., Andersen, B.G., Schwartz, R., Chinn, T.J.H., Doughty, A.M., 2012. Regional climate control of glaciers in New Zealand and Europe during the pre-industrial Holocene. Nat. Geosci. 5, 627–630.
Raper, S.C.B., Braithwaite, R.J., 2009. Glacier volume response time and its links to climate and topography based on a conceptual model of glacier hypsometry. Cryosphere Discuss. 3, 243–275.

Reimer, P.J., et al., 2009. INTCAL09 and MARINE09 radiocarbon age calibration curves, 0–50,000 years cal BP. Radiocarbon 51, 1111–1150.
Reyes, A.V., Wiles, G.C., Smith, D.J., Barclay, D.J., Allen, S., Jackson, S., Larocque, S., Laxton, S., Lewis, D., Calkin, P.E., Clague, J.J., 2006. Expansion of alpine glaciers in Pacific North America in the first millennium A.D. Geology 34, 57–60. http://dx.doi.org/10.1130/G21902.1.
Robock, A., 2000. Volcanic eruptions and climate. Rev. Geophys. 38, 191–219.
Schaefer, J.M., Denton, G.H., Kaplan, M., Putnam, A., Finkel, R.C., Barrell, D.J.A., Andersen, B.G., Schwartz, R., Mackintosh, A., Chinn, T., Schlüchter, C., 2009. High-frequency Holocene glacier fluctuations in New Zealand differ from the northern signature. Science 324, 622–625.
Seton-Karr, H.W., 1887. Shores and Alps of Alaska. Ballantyne Press, London, p. 248.
Shennan, I., Bruhn, R., Plafker, G., 2008. Multi-segment earthquakes and tsunami potential of the Aleutian megathrust. Quat. Sci. Rev. 28, 7–13.
Shreve, R.L., 1966. Sherman landslide, Alaska. Science 154, 1639–1643.
Steinhilber, F., Beer, J., Fröhlich, C., 2009. Total solar irradiance during the Holocene. Geophys. Res. Lett. 36, L19704. http://dx.doi.org/10.1029/2009GL040142.
Stuiver, M., Reimer, P.J., 1993. Extended ^{14}C database and revised CALIB radiocarbon calibration program. Radiocarbon 35, 215–230.
Tarr, R.S., Martin, L., 1914. Alaskan Glacier Studies. The National Geographic Society, Washington, p. 498.
Tuthill, S.J., Field, W.O., Clayton, L., 1968. Postearthquake studies at Sherman and Sheridan glaciers. In: The Great Alaska Earthquake of 1964 – Hydrology. National Academy of Sciences Publication 1603, pp. 318–328.
Vierek, L.A., 1967. Botanical dating of recent glacial activity in western North America. In: Wright Jr., H.E., Osburn, W.H. (Eds.), Arctic and Alpine Environments. Indiana University Press, Bloomington, Indiana, pp. 189–204.
Vincent, C., Le Meur, E., Six, D., 2005. Solving the paradox of the end of the Little Ice Age in the Alps. Geophys. Res. Lett. 32, L09706. http://dx.doi.org/10.1029/2005GL022552.
Wentworth, C.K., Ray, L.L., 1936. Studies of certain Alaskan glaciers in 1931. Bull. Geol. Soc. Am. 47, 879–934.
Wiles, G.C., Calkin, P.E., 1994. Late Holocene, high-resolution glacial chronologies and climate, Kenai Mountains, Alaska. Geol. Soc. Am. Bull. 106, 281–303.
Wiles, G.C., D'Arrigo, R.D., Jacoby, G.C., 1998. Gulf of Alaska atmosphere–ocean variability over recent centuries inferred from coastal tree-ring records. Clim Change 38, 289–306.
Wiles, G.C., Barclay, D.J., Calkin, P.E., 1999. Tree-ring-dated Little Ice Age histories of maritime glaciers from western Prince William Sound, Alaska. Holocene 9, 163–173.
Wiles, G.C., D'Arrigo, R.D., Villalba, R., Calkin, P.E., Barclay, D.J., 2004. Century-scale solar variability and Alaskan temperature change over the past millennium. Geophys. Res. Lett. 31, L15203. http://dx.doi.org/10.1029/2004GL020050.
Wiles, G.C., Barclay, D.J., Calkin, P.E., Lowell, T.V., 2008. Century to millennial-scale temperature variations for the last two thousand years inferred from glacial geologic records of southern Alaska. Global Planet. Change 60, 115–125. http://dx.doi.org/10.1016/j.gloplacha.2006.07.036.
Wilson, R., Wiles, G., D'Arrigo, R., Zweck, C., 2007. Cycles and shifts: 1300 years of multi-decadal temperature variability in the Gulf of Alaska. Clim. Dyn. 28, 425–440. http://dx.doi.org/10.1007/s00382-006-0194-9.
Winkler, G.R., Plafker, G., 1993. Geologic Map of the Cordova and Middleton Island Quadrangles, Southern Alaska. In: U.S. Geological Survey Miscellaneous Investigations Series. Map I-1984, 1 Sheet.
Zander, P., Kaufman, D., Kuehn, S., Wallace, K., Anderson, R., 2013. Early and late Holocene glacial fluctuations and tephrastratigraphy, Cabin Lake, Alaska (3-Jun-2013) (submitted for publication). J. Quat. Sci..